INSTITUTE OF PHYSICS PUBLISHING JOURNAL OF PHYSICS: CONDENSED MATTER

J. Phys.: Condens. Matter **18** (2006) 10165–10177 doi:10.1088/0953-8984/18/45/005

A molecular dynamics study of hydration and dissolution of NaCl nanocrystal in liquid water

Yong Yang[1], **Sheng Meng**[2] **and E G Wang**[1,3]

[1] Institute of Physics, Chinese Academy of Sciences, Box 603, Beijing 100080, People's Republic of China
[2] Department of Physics and Division of Engineering and Applied Sciences, Harvard University, Cambridge, MA 02138, USA
[3] Fritz-Haber-Institut der Max-Planck-Gesellschaft, Faradayweg 4-6, D-14195 Berlin, Germany

Received 17 July 2006, in final form 14 September 2006
Published 26 October 2006
Online at stacks.iop.org/JPhysCM/18/10165

Abstract

The interfacial structure and dynamical processes of a NaCl nanocrystal in liquid water have been studied in detail through classical molecular dynamics simulations. Before dissolution, the radial distribution of water molecules around the nanocrystal exhibits a multi-shell structure at the solid–liquid interface. The thermodynamic properties of the hydrated NaCl nanocrystal were studied by calculating its kinetic energy distribution and vibrational spectrum, which show a good agreement with experiment. The characteristics of NaCl dissolution dynamics, such as ion sequence, dissolved species, dissolution force, and dynamical role of water molecules during the dissolution were further investigated based on the statistical analysis. An ion sequence of Cl^-, Na^+, Cl^- ... and intermitted neutral pairs taking place from corner then ledge sites is preferred in NaCl dissolution processes.

(Some figures in this article are in colour only in the electronic version)

1. Introduction

According to Arrhenius' theory of electrolytic dissociation [1], a strong electrolyte is a compound that will completely ionize or dissociate into ions when dissolved in water. Such examples include the most common salt: when NaCl is placed in water, it should completely dissociate into Na^+ and Cl^- ions.

However, this point of view contrasts with some recent experimental findings for salt solution. Raman spectroscopy has suggested the presence of clusters in $NaNO_3$ [2], KH_2PO_4, and $(NH_4)H_2PO_4$ [3] aqueous salt solutions. Using dynamical light scattering, Georgalis *et al* [4] observed directly the existence of NaCl, $(NH_4)_2SO_4$, and sodium citrate submicrometre size clusters at room temperature in both supersaturated and undersaturated aqueous solutions. Their findings imply that in aqueous solutions simple electrolytes, such as NaCl, aggregate even at moderate concentrations, and make it necessary to understand the dynamical hydration

process of salt nanoclusters in liquid water, which is also important for the dissolution mechanism in aqueous solutions. On the other hand, the synthesis of nanocrystals [5] from solution requires a molecular-level study for the kinetic process occurring in the liquid–solid interface. The hydration process of a NaCl nanocrystal in liquid water can serve as a good prototype for the purpose.

Besides experiments, computational simulations are receiving great interest in the way of understanding a number of processes that take place in solutions at molecular level. For example, molecular dynamics (MD) simulations based on empirical potentials and model systems have revealed dynamical processes at the liquid–solid interface [6, 7] as well as the effect of water in the early stage of dissolution for NaCl nanocrystals [8], and observed initial events for NaCl nucleation in supersaturated solutions [9], or from an evaporating salt solution [10], or nucleation from the melting state of NaCl cluster [11]. Even so, little is known about the pre-solvation state of the NaCl nanocrystals and the detailed dissolution mechanism.

It is the aim of this paper to present a comprehensive study of the hydration and dissolution dynamics of NaCl nanocrystals in liquid water, using classical molecular dynamics simulations. The ratio between numbers of NaCl units and water molecules, $N(NaCl)/N(H_2O)$, corresponds to an undersaturated NaCl solution. In our early study [8], the ion sequence of $Cl^-, Na^+, Cl^-, \ldots$, dissolution sites at crystal corners and the directional preference of dissolved ions were found. Here we extend our simulations from one trajectory [8] to a number of different initial configurations, and to a much longer simulation time for some of them. Detailed statistical analysis based on the massive MD trajectories has been performed. We found that the number of water molecules in the hydration shell of the nanocrystal fluctuates significantly. The radial distribution of water molecules around the nanocrystal shows clearly three peaks, corresponding to the main feature of the hydration structure of the NaCl nanocrystal. The thermal motions of the nanocrystal were investigated by comparing kinetic energy distribution of inner and surface ions, and by calculating the vibration spectra. The dynamical roles that water plays during the dissolution were further studied by analysing its thermodynamical properties in the NaCl solution.

2. Computational methods

Classical molecular dynamics was performed using the AMBER 6 package [12]. The simulation supercell, shown in figure 1(a), consists of 32 Na^+ and 32 Cl^- ions in a cubic nanocrystal (with $\sim$11.3 Å in each direction) surrounded by 625 water molecules in the liquid state with a density of $\sim$1 g cm^{-3}. The interface between solid and liquid has thus six equivalent (100) faces. The water–water interaction is described by the TIP3P model [13], while the ion–ion and ion–water interactions are described by the PARM94 force field provided by AMBER 6 [12]. The system used for modelling the hydration process of the nanocrystal was prepared with an initial equilibration at $\sim$300 K for 150 ps and then heated up to $\sim$350 K for 100 ps, before the production run. The temperature of 350 K was chosen to enhance the dissolution process. Harmonic restraints on the NaCl crystal coordinates were used during the equilibration procedure. The initial simulation box was 27.86 Å $\times$ 27.88 Å $\times$ 27.50 Å in size, which fluctuates within 0.5 Å during the NTP (canonical ensemble with constant pressure) simulations. The other systems used for statistical study of the dissolution were equilibrated for at least 250 ps before MD simulations at $\sim$350 K. A periodic boundary condition was applied. The particle mesh Ewald method [14, 15] was used to calculate the electrostatic energies and forces, and the van der Waals interactions. The real space part of the Ewald sum was truncated at 10 Å. A time step of 0.5 fs was used, and the OH vibrations were frozen using the SHAKE algorithm [16]. The temperature and pressure were controlled by a Berendsen's thermostat

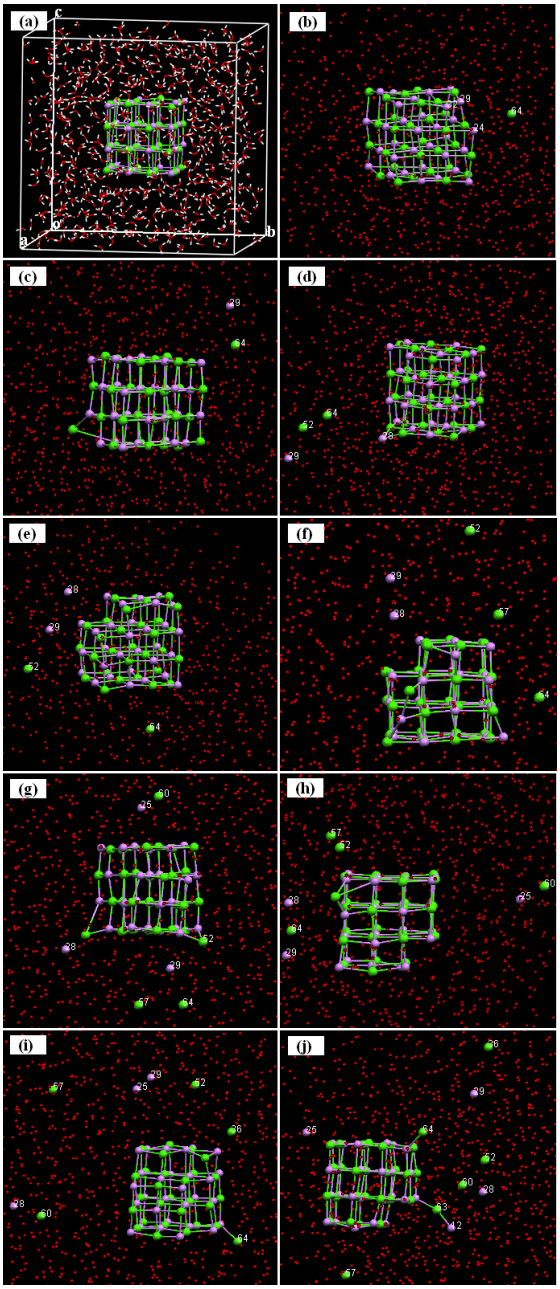

Figure 1. (a) The unit cell used in the simulations with 32 NaCl pairs and 625 water molecules. The Na^+ and Cl^- ions are represented by purple (small) and green (large) balls, respectively. Water molecules are represented by bended sticks (small for hydrogen and large for oxygen). (b)–(j) Snapshots in an MD simulation at $t = 241.635$ ps (b), 369.9 ps (c), 2013 ps (d), 2088 ps (e), 2108 ps (f), 2450 ps (g), 2475 ps (h), 3297.5 ps (i), 3625 ps (j), showing a dissolution sequence of Cl^-, Na^+, Cl^-, Na^+ . . .. For clarity, the hydrogen atoms are not shown in the snapshots.

and barostat [17], respectively, towards the target values of 350 K and 1 bar. For simulations longer than 1.8 ns, the velocities of the water molecules and the NaCl nanocrystal were reset

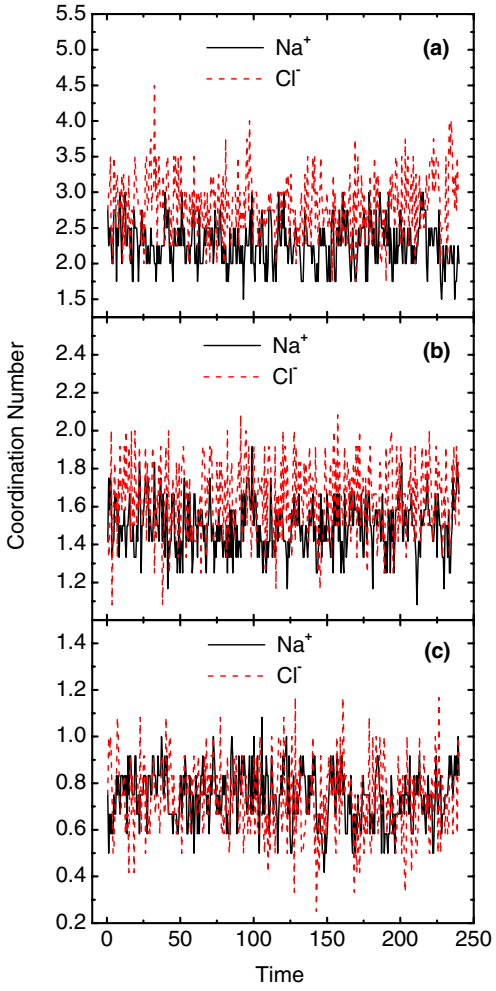

Figure 2. Time evolution of the averaged water coordination number (CN) around the nanocrystal: (a) corner sites; (b) edge sites; (c) NaCl(100) surfaces of the NaCl nanocrystal.

by a Maxwellian distribution at 350 K while the ionic configurations were kept for continuous simulations.

The validity of the model potentials used in AMBER was tested by comparing with *ab initio* calculations for Na^+ $(H_2O)_n$ and Cl^- $(H_2O)_n$ ($n = 1$–3) clusters and water adsorption on the NaCl(100) surface. A good agreement was found [8]. In addition, the cohesive energy of bulk NaCl is calculated by AMBER to be -188.7 kcal mol^{-1} ($\sim$8.2 eV per ion pair), very close to the -185.5 kcal mol^{-1} given by experiment [18].

3. Results and discussion

3.1. Before dissolution

3.1.1. Water distribution around the nanocrystal. The distribution of the water molecules at the H_2O/NaCl interface plays a central role in the dissolution and crystallization process. Figure 2 shows the time evolution of the average water coordination number (CN) of the

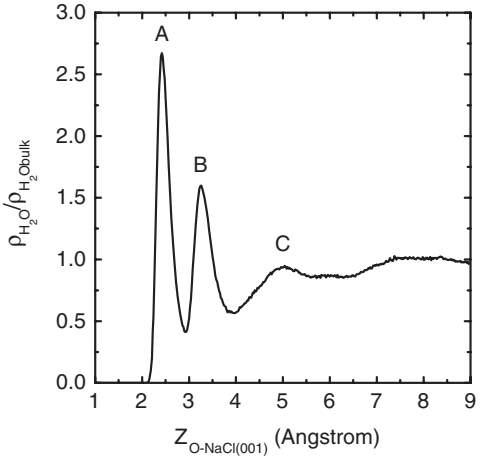

Figure 3. Radial density of water molecules around the nanocrystal, as a function of distance to the surface of the nanocrystal.

surface Na^+ and Cl^- ions at the non-equivalent sites (corner, edge, NaCl(100) surface) of the nanocrystal. The CN is defined by counting the number of water molecules within a sphere, i.e., $r_{Cl-O} \leqslant 3.90$ Å, and $r_{Cl-H} \leqslant 3$ Å for Cl^- and $r_{Na-O} \leqslant 3.25$ Å for Na^+ respectively, according to the hydration radii of Na^+ and Cl^- ions in aqueous solution. In the solution state, these numbers correspond to the number of water molecules in the first hydration shell of the Na^+ and Cl^- ions. The statistics were performed for the first 240 ps, because the dissolution process started at ∼232 ps, and took about 15 ps to dissolve the first corner ion. From figures 2(a) to (c), the water CN shows a general tendency of decreasing, due to the decrease of water–NaCl contact angle ($\sim\frac{7}{8} \times 2\pi$, $\frac{3}{4} \times 2\pi$, $\frac{1}{2} \times 2\pi$ for corner, edge, NaCl(100), respectively). On average, the water CNs of Cl^- at corner and edge sites are larger than the corresponding numbers of Na^+. The water CN of the two type of ions appears to have the same average value at the NaCl(100) surface (figure 2(c)).

The average water CN for the surface ions during the first 240 ps is ∼2.3 H_2O/NaCl unit, which can be regarded as the first hydration shell of the nanocrystal. One can find that the water CN fluctuates with considerable amplitude during the hydration process, and the water CN of Cl^- exhibits larger fluctuation than that of Na^+. As we will show below, this is the microscopic driving force for the dissolution of the nanocrystal in liquid water.

To explore the statistical properties, the density distribution of water molecules around the nanocrystal during the first 232 ps was investigated. In the following discussion, we use the distance to the surface of the nanocrystal as the variable. However, it is difficult to calculate the average water density at the solid–liquid interface accurately, due to the fact that the surface area and the volume of the nanocrystal fluctuate with small amplitude during the MD simulations. By neglecting the fluctuation in the shape and volume of the nanocrystal, the average radial density, which is defined by the division between the number of water molecules in a thin shell copying the crystal surface with the shell thickness of δZ, can give us valuable information, as shown in figure 3. The water density is rescaled with reference to the density of bulk water. Three peaks appear in the curves. In fact, the peaks, marked as A, B, and C in figure 3, are correlated with the local structure of water in the H_2O/NaCl interface region. The first peak, which is located at a distance of ∼2.40 Å to the surface of the nanocrystal, corresponds to the first water layer that covers the NaCl(100) surface. This means that the average water (O atom)–NaCl(100) separation is ∼2.40 Å. Similarly, the second peak ($Z_{O-NaCl(100)} \sim 3.27$ Å)

and the third peak ($Z_{\mathrm{O-NaCl(100)}} \sim 5.00$ Å) correspond to the second and the third hydration layer of the NaCl nanocrystal, respectively. The minimum of the third peak sits at ∼5.5 Å, which indicates the presence of an ordered water network at $Z_{\mathrm{O-NaCl(100)}} \leqslant 5.5$ Å. This result is supported by recent experimental observations at the water–NaCl(100) interface [19]. A similar result was reported by MD simulations at the water–NaCl(100) interface [20], although the height of peaks shows a small difference, and the position of the third peak differs by ∼1 Å, which may result from the finite crystal size in our calculation, while a periodic infinite NaCl(100) slab (in the X, Y plane) was used in the simulation there [20]. In figure 3, the water density remains almost constant at ∼0.87 g cm^{-3} at distance $Z_{\mathrm{O-NaCl(100)}} = 5.5$–6.5 Å, then increases to the bulk water density at ∼7.5 Å. This is the transition region from interface water to bulk water. As the distance $Z_{\mathrm{O-NaCl(100)}}$ increases to more than 7.5 Å, the density of water molecules approaches the bulk density, which is ∼1 g cm^{-3}; no peaks are observed.

3.1.2. Thermal motions of the NaCl nanocrystal. The nanocrystal translates and rotates in liquid water due to thermal motions of the Na^+ and Cl^- ions and energy exchange with water. We have studied the kinetic energy distribution of ions inside and outside the crystal at four typical positions: inner site, the NaCl(100) surface, edge site, and corner site.

The calculation was carried out for the first 232 ps, before the dissolution started. Based on a Maxwell velocity distribution, the kinetic energy distribution of single particle is (see the appendix):

$$p(E_{\mathrm{k}}) = 2\pi\left(\frac{1}{\pi k_{\mathrm{B}}T}\right)^{\frac{3}{2}}\sqrt{E_{\mathrm{k}}}\,\mathrm{e}^{-\frac{E_{\mathrm{k}}}{k_{\mathrm{B}}T}}. \tag{1}$$

The statistical distribution of $p(E_{\mathrm{k}})\mathrm{d}E_{\mathrm{k}}$ is shown in figure 4. The shapes of the kinetic energy distribution curves are independent of the mass of the particles and the force field that the particle experiences.

The maxima of the curves are determined as $\frac{\mathrm{d}p(E_{\mathrm{k}})}{\mathrm{d}E_{\mathrm{k}}} = 0$, and the positions of the peaks are $E_{\mathrm{km}} = \frac{1}{2}k_{\mathrm{B}}T$. At $T = 350$ K, $E_{\mathrm{km}} \approx 0.35$ kcal mol^{-1}, in good agreement with the peak positions shown in figure 4. The average kinetic energies of all the configurations are located at ∼1 kcal mol^{-1}. This result is reasonable. According to statistical mechanics, the average kinetic energy of N_{A} particles at 350 K is calculated to be $\bar{E}_{\mathrm{k}} = \frac{3}{2}N_{\mathrm{A}}k_{\mathrm{B}}T = 1.04$ kcal mol^{-1}. All these results clearly indicate that the systems in our simulation are in thermal equilibrium states.

Another important aspect of thermal motions is the vibrational spectrum, which can be obtained through Fourier transform of the velocity–velocity autocorrelation function:

$$C_{\mathrm{vv}}(\omega) = \frac{1}{N}\sum_{I=1}^{N}\int \mathrm{d}t[\vec{V}_I(t)\cdot\vec{V}_I(0)]\mathrm{e}^{\mathrm{i}\omega t}. \tag{2}$$

The calculated spectra for the NaCl nanocrystal and for the liquid water around it are shown in figure 5. The trajectories used in our spectra analysis cover 10 ps with 20 000 configurations. The spectra for the NaCl nanocrystal and the liquid water are shown in figures 5(a) and (b), respectively, corresponding to the translational and rotational motions of the NaCl nanocrystal and the water molecules. Four inequivalent positions of the nanocrystal, i.e., the corner sites, the edge sites, the (100) face sites and the bulk inner sites, are considered here. Because of the mass difference of Na^+ and Cl^- ions, there should be at least $2 \times 4 \times 3$ different modes in the spectra, which are included in figure 5(a). Suppose that the interactions between the ions of NaCl nanocrystal satisfy the harmonic approximation. Then, the vibration modes can be classified by the bonding sites and the mass of the ions. The relation between the vibration

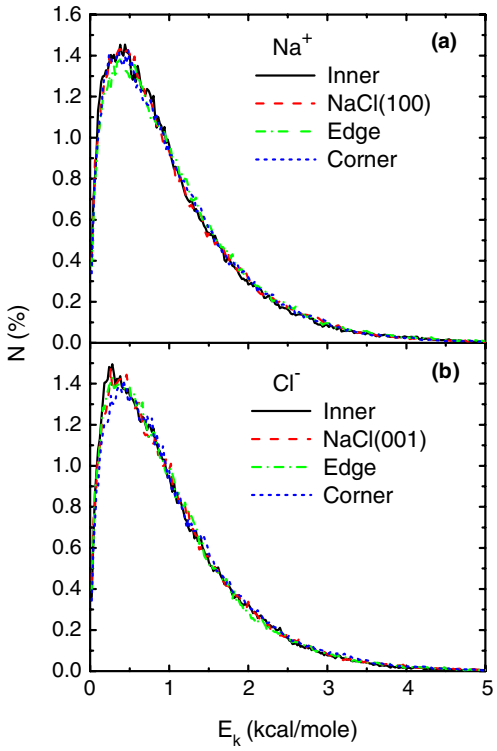

Figure 4. Statistical distribution of the kinetic energies of the single Na^+ (a) and Cl^- (b) ions at different sites of the NaCl nanocrystal. Here $N(\%) = p(E_k)\mathrm{d}E_k$. Each calculation was done for the first 232 ps with 464 000 configurations. The data points are sampled with an energy interval of 0.02 kcal mol^{-1}.

frequency ω and the mass of the ions M is

$$\omega \propto \frac{1}{\sqrt{M}}. \tag{3}$$

Therefore,

$$\frac{\omega_{Na}}{\omega_{Cl}} = \sqrt{\frac{M_{Cl}}{M_{Na}}} \approx 1.24. \tag{4}$$

The positions of the 24 typical peaks in figure 5(a), and their classification according to equation (4), are listed in table 1. One can see the simulated vibrational frequencies that are related to the harmonic eigenmotions of the Na^+ and Cl^- ions satisfy the relation given in equation (4) quite well, except for frequencies lower than 60 cm^{-1}. The modes located between 152 and 213 cm^{-1} are comparable with previous infrared spectra of NaCl crystal [21], indicating the motions of the inner ions of the nanocrystal.

The spectrum of water molecules is far more complex—with vibrational overtones and combinations of librations (i.e., frustrated rotations, such as rocking, wagging, and twisting motions), due to the presence of hydrogen bonds. It shows the main feature of a broad peak at 450 cm^{-1} and a shoulder at 800 cm^{-1}. They have been measured in inelastic neutron scattering and infrared adsorption spectroscopy of liquid water (centred at 580 and 806 cm^{-1}, respectively) [22–24]. The modes centred at 72, 165, 205, 391, 635, and 676 cm^{-1} are also

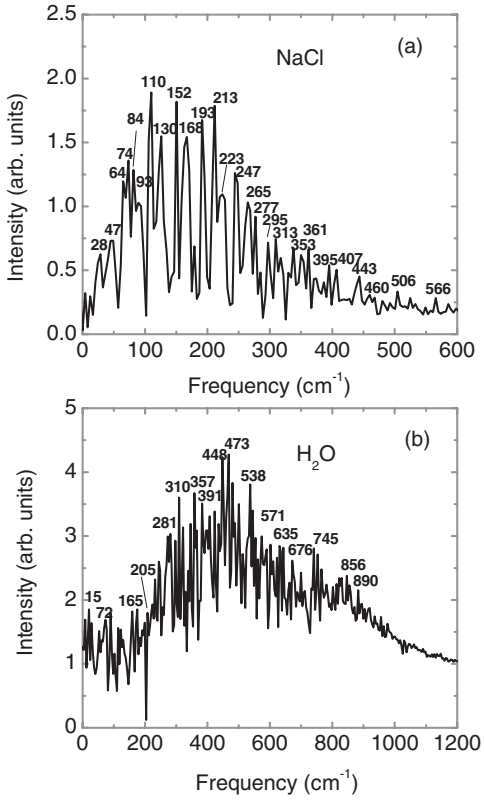

Figure 5. Calculated vibrational spectra of the NaCl nanocrystal (a) and liquid water around the nanocrystal (b).

Table 1. The 24 typical modes in the vibrational spectra of NaCl nanocrystal in water (figure 5(a)). The first two lines are the vibrational modes calculated by MD simulations, which are related to the harmonic eigenmotions of Na^+ and Cl^- ions, respectively. The third line is the corresponding harmonic eigenmodes related to the motions of Cl^- ions, which are obtained via equation (4) in the text and the vibrational modes related to Na^+ (the first line). The unit for frequency is cm^{-1}.

Assignment of spectra	ω_1	ω_2	ω_3	ω_4	ω_5	ω_6	ω_7	ω_8	ω_9	ω_{10}	ω_{11}	ω_{12}
Na^+ simulation	566	506	443	395	361	277	265	247	168	152	93	84
Cl^- simulation	460	407	353	313	295	223	213	193	130	110	74	64
Cl^- harmonic	456	408	357	319	291	223	214	199	135	123	75	68

in agreement with available theoretical [25] and experimental results [26]. The shift of the peaks from bulk water values (e.g., 473 cm^{-1} (figure 5(b)) versus 580 cm^{-1} [22, 23]), and the emergence of new peaks (e.g., 281, 310, 538 cm^{-1} in figure 5(b)) reflect the influence of the NaCl nanocrystal on the vibrations of water. Because the OH vibrations are frozen in our simulations, intramolecular vibration modes are absent in the spectra.

3.2. Dissolution dynamics

3.2.1. Ion sequences and dissolution species. We now discuss the dissolution dynamics of the NaCl nanocrystal. All the MD simulations were run at ∼350 K to facilitate the dissolution

process. The first atomic feature is the ion sequence during dissolution. A typical trajectory is shown in figure 1, where ion dissolution starts at ∼232 ps. For convenience, we tagged the Na^+, Cl^- ions with integers ranging from 1–64: 1–32 for Na^+ and 33–64 for Cl^-. The first ion that dissolves into water is one of the corner site Cl^- ions, marked as Cl^{64} in figure 1(b), and the second is one of its neighbour Na^+ ions, Na^{29}, shown in figure 1(c). The third one is Cl^{52} (figure 1(d)), and the fourth one is Na^{28} at 2088 ps (figure 1(e)). At this stage, a ledge of the NaCl nanocrystal is completely dissolved. However, the dissolution process continues to proceed with the fifth ion, Cl^{57}, which dissolves at $t \sim 2108$ ps (figure 1(f)). At $t \sim 2430$ ps, Na^{25} and Cl^{60}, which are bonded at the edge site of the nanocrystal, dissolve into water almost simultaneously, in the form of a Na^+–Cl^- ion pair (figures 1(g) and (h)). An ion sequence of Cl^-, Na^+, Cl^-, Na^+, Cl^-, ... was therefore observed for the dissolution of the first seven ions during the 2.5 ns MD simulations. This reveals both separated and charged ions (Na^+ or Cl^-), and neutral ion pairs can be dissolved in liquid solution. However, the latter happens at much smaller probabilities as in our simulation.

As the NaCl dissolution further proceeds, the first dissolved ion, Cl^{64}, attaches to the undissolved part of the nanocrystal on a different site. Another corner ion, Cl^{36}, then starts to leave the crystal (figure 1(i)) at $t \sim 3297.5$ ps. About 327.5 ps later, one of its neighbours, Na^{12}, breaks two Na–Cl bonds and shows a tendency of dissolving (figure 1(j)). Its neighbour Cl^{63} is also dragged out with a Na–Cl bond sticking outwards from the nanocrystal. Indeed, both of them are dissolved into water in continuous simulations.

The dissolution process discussed above shows a tendency of maintaining the least charge separation of the nanocrystal: one anion is followed by or coupled to one cation. This also explains our observation that the dissolved species can be either single charged ions or neutral ion pairs, though the latter may have less probability and shorter lifetime than the former. In our simulations, we found that after the corner ion of the edge is dissolved, it has a high tendency to dissolve the Na^+ and Cl^- at the edge in the form of bound Na^+–Cl^- pairs, and the dissolution was continued by corner ions and their nearest neighbours with the opposite charge. We expect that this microscopic equilibration can be extended to further dissolution of the nanocrystal, until the electrostatic forces contributed from the remaining part of the nanocrystal are negligible compared to the hydration forces of water.

Because the dissolution process is mainly a statistical process, it is important to look at the statistical properties of the dissolution processes. Aiming at obtaining statistical data, we did nine different MD simulations of dissolution dynamics with different starting configurations. Our results show that six dissolution events started with Cl^- ions, and three dissolution events started with Na^+ ions. As for the initial dissolution sites, eight dissolution events started from corner sites, and one from the edge site. This supports the picture in our previous study [8], that the Cl^- ions tend to have better chance to dissolve into water than Na^+ ions, and dissolution events are more likely to begin with corner sites.

3.2.2. Dissolution forces. In most trajectories, the dissolution of the corner Na^+ and Cl^- ions were started by breaking two of the three ionic bonds almost simultaneously, and the third bond was broken several picoseconds later, which leads to a directional preference in the early dissolution trajectories, i.e., $[11\bar{1}]$ rather than [111]. This can be understood from the difference in the energy barrier of removing one ion from the corner site in the two directions [8], shown in figure 6. For illustration, we will further discuss two dissolution events and their driving forces in the prototype trajectory (figures 1(b) and (c)), which started at ∼232 ps for Cl^{64}, and ∼324 ps for Na^{29}.

Figure 7 shows the forces acting on the two ions during their dissolution. Dissolution forces come from the electrostatic hydration forces of the nanocrystal. The absolute values of

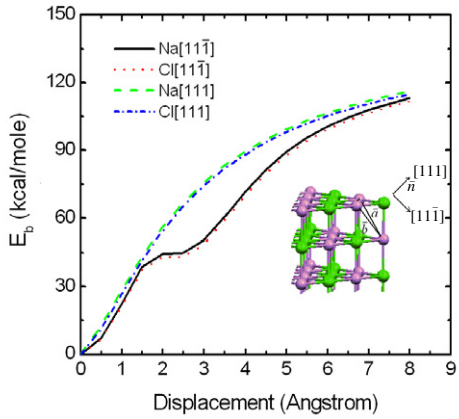

Figure 6. The energy barrier for removing one Na^+ (Cl^-) from the corner site of a pure NaCl crystal into vacuum along the [11$\bar{1}$] and [111] directions, respectively. The local frame of reference used in our calculations is constructed by the vectors $\vec{a}$, $\vec{b}$, $\vec{n}$.

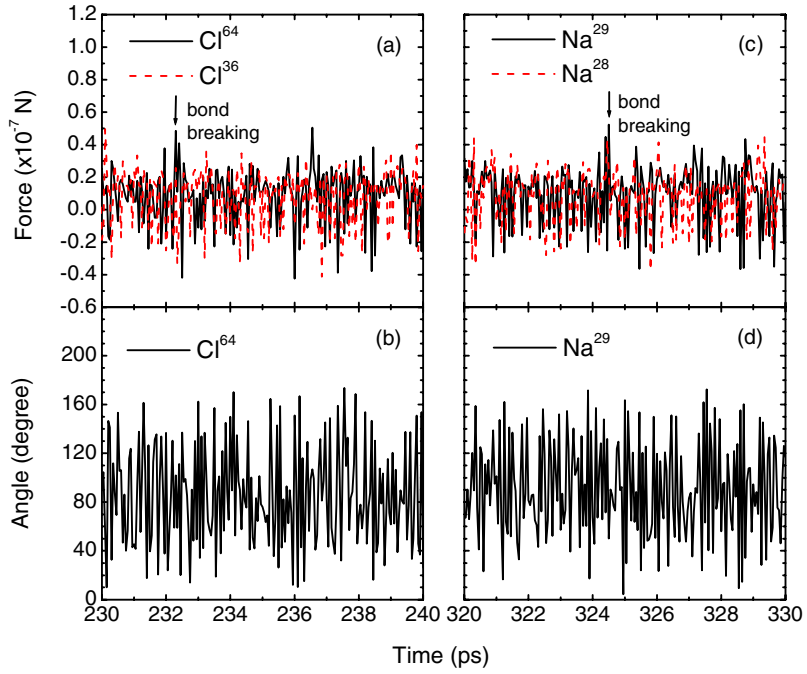

Figure 7. Evolution of the force magnitudes acting on the dissolved Cl^{64} (left panels) and Na^{29} (right panels), and the angles formed between the forces and the facet normal $\vec{n}$ (see figure 6). The forces on the other two corner ions, Cl^{36} and Na^{28}, which do not dissolve during this period, are also shown for comparison. Arrows indicate the events when two Na–Cl bonds were broken during the dissolution process.

the forces were calculated using Newton's second law of motion, through the difference of the velocities between the present and next steps. The sign of the force is defined as follows: if the

force points inside the crystal, the sign is negative; if it points away from the crystal, the sign is positive. Because the nanocrystal translates and rotates in liquid water, we used a local frame as reference to describe the motions of the corner ions, and to calculate the directions of the forces. The local reference frame is defined by the crystal facet and its normal $\vec{n}$ (figure 6). The magnitudes of instant forces acting on the dissolved ions are shown in figures 7(a) and (c), and their directions measured by the angles between the forces and the normal of the facet are given in figures 7(b) and (d). The force on the other two undissolved corner ions, Cl^{36} and Na^{28}, is also shown for comparison.

In figure 7, the dissolution forces oscillate strongly during the dissolution processes for both Cl^- and Na^+ ions. The direction of the forces can change quickly from pointing inside to pointing outside the crystal. At the onset of the ion dissolution (indicated by vertical arrows), the forces on the dissolved ions increase significantly, pointing outward with the angle of $\sim 90°$. This corresponds to the breaking of two Na–Cl bonds simultaneously along the $[11\bar{1}]$ directions, consistent with our previous discussions [8].

In order to study the ion motions, we calculated the velocities of the Na^+ and Cl^-. We determined the angle between the velocity of the dissolved ions and the normal of the crystal facet $\vec{n}$ from the following equation,

$$\cos\phi = \frac{\vec{v} \cdot \vec{n}}{|\vec{v}| \cdot |\vec{n}|}. \tag{5}$$

Just before their dissolution, the average angle ϕ for Cl^{64} (from 230 to 240 ps) is 91.5° and for Na^{29} (from 320 to 330 ps) is 85.4°. Both are close to 90°. Statistical distribution of the angle ϕ for the dissolved ions reveals that the maxima of the appearing times of ϕ are located at $\sim 90°$. This indicates that, at the early stage of salt dissolution, the dissolved ions would move along the pathway along $[11\bar{1}]$ and equivalent directions, which is an averaged and the most probable direction, rather than [111] (corresponding angle $\phi = 0$). The discussion based on figure 6 is in fact the averaged effect of the path selection.

3.2.3. Water dynamics around the nanocrystal. After an ion is dissolved into water, the other ions at equivalent crystal sites remain in the crystal. The dissolution process is accompanied with a sharp increase of the water coordination numbers, that is, the density fluctuations of the water molecules around the ions. For instance, the number of water molecules in the first hydration shell of corner site Cl^- can vary from 0 to 7. This is actually the microscopic reason for the calculated dissolution forces in figure 7, which finally dissolves the NaCl nanocrystal. The fluctuations are further studied in our simulations of liquid water (modelled by 625 water molecules in a periodic box) at 350 K. The local density of the water molecules shows a broad distribution and obeys the Gaussian distribution.

3.3. Ions after dissolution

As described above and shown in figure 1, the ions from the NaCl nanocrystal enter the water when it starts to dissolve. They exist mainly as separated single Na^+ or Cl^- ions and form three-dimensional hydration shells in the solution. Some neutral NaCl pairs are also possible in the solution. The ion pair breaks into separate Na^+ and Cl^- ions, which are more stable hydration structures in liquid water. During the onset of the crystal dissolution process, dissolved Na^+ and Cl^- ions in the solution could also re-adsorb on the crystal surface, as observed in our simulation at $t \sim 3298$ ps. These surface-bound ions also play an important role during the dissolution process to maintain the charge neutrality of the nanocrystal, and help to dissolve other strongly bound ions with the same charge which otherwise do not dissolve directly.

4. Conclusions

Based on molecular dynamics simulations, the dynamical and statistical properties of a NaCl nanocrystal in liquid water were investigated.

Before dissolution, the number of water molecules in the first hydration shell of the nanocrystal is found to fluctuate with significant amplitude, and the Cl^- ion usually accommodates more water molecules around it than Na^+ ion does. The radial distribution of water molecules shows three peaks around the nanocrystal, which is a reflection of the main feature of the hydration shell of the nanocrystal. The kinetic energy distribution of the single ion at different positions is calculated. The vibrational spectra of the nanocrystal and its surrounding water were calculated through the Fourier transformation of velocity–velocity auto-correlation functions, and were compared with the existing experiments.

We have further discussed the dissolution dynamics of the nanocrystal in liquid water. Our statistical analysis showed that most dissolution events started from corner sites, though an event that started from an edge site was also observed. Most ions get dissolved into water by breaking two of the three ionic bonds simultaneously, along a most probable direction of $[11\bar{1}]$. Once an ion is dissolved, it is often followed by a counter ion, maintaining the minimal of charge separation. We expect that the ion sequence of Cl^-, Na^+, Cl^-, Na^+, ... observed in our MD simulations can be tested by future experiment. After dissolution, some ions can re-adsorb on the nanocrystal surface, which shows the influence on the dissolution of the other ions.

Acknowledgments

The work was partly supported by the NSF of China and the Humboldt Research Award (EGW). We acknowledge Shiwu Gao and Lifang Xu for many helpful discussions.

Appendix

The velocity distribution function of a single particle is

$$f(v) = 4\pi\left(\frac{m}{2\pi k_B T}\right)^{\frac{3}{2}} v^2 e^{-\frac{m}{2k_B T}v^2}. \tag{A.1}$$

Let

$$C_1 = 4\pi\left(\frac{m}{2\pi k_B T}\right)^{\frac{3}{2}}, \qquad C_2 = \frac{m}{2k_B T}.$$

For a kinetic energy distribution, the variable changes to $E_k = \frac{1}{2}mv^2$, its inverse function is $v(E_k) = \sqrt{\frac{2E_k}{m}}$, and its distribution function is

$$p(E_k) = f(v(E_k))v'(E_k) = C_1\frac{2E_k}{m}e^{-C_2\frac{2E_k}{m}}\frac{1}{\sqrt{2mE_k}} = C_1\sqrt{\frac{2E_k}{m^3}}e^{-C_2\frac{2E_k}{m}}.$$

Making use of the values of C_1 and C_2, we get

$$p(E_k) = f(v(E_k))v'(E_k) = C_1\frac{2E_k}{m}e^{-C_2\frac{2E_k}{m}}\frac{1}{\sqrt{2mE_k}} = 4\pi\left(\frac{1}{2\pi k_B T}\right)^{\frac{3}{2}}\sqrt{2E_k}e^{-\frac{E_k}{k_B T}},$$

$$p(E_k) = 2\pi\left(\frac{1}{\pi k_B T}\right)^{\frac{3}{2}}\sqrt{E_k}e^{-\frac{E_k}{k_B T}}. \tag{A.2}$$

This is the kinetic energy distribution of a single particle in a thermal equilibration system.

References

[1] Arrhenius S 1903 *Nobel Lecture 11 December*
[2] Rusli I T, Schrader G L and Larson M A 1989 *J. Cryst. Growth* **97** 345
[3] Cerreta M K and Berglund K A 1987 *J. Cryst. Growth* **84** 577
[4] Georgalis Y, Kierzek A M and Saenger W 2000 *J. Phys. Chem.* B **104** 3405
[5] Wang X, Zhuang J, Peng Q and Li Y D 2005 *Nature* **437** 121
[6] Bahadur R, Russell L M, Alavi S, Martin S T and Buseck P R 2006 *J. Chem. Phys.* **124** 154713
[7] Monson P A and Kofke D A 2000 *Adv. Chem. Phys.* **115** 113
[8] Yang Y, Meng S, Xu L F, Wang E G and Gao S W 2005 *Phys. Rev.* E **72** 012602
[9] Zahn D 2004 *Phys. Rev. Lett.* **92** 040801
[10] Mucha M and Jungwirth P 2003 *J. Phys. Chem.* B **107** 8271
[11] Huang J F, Zhu X L and Bartell L S 1998 *J. Phys. Chem.* A **102** 2708
[12] Case D A, Pearlman D A, Caldwell J W, Cheatham T E III, Ross W S, Simmerling C, Darden T, Merz K M, Stanton R V, Cheng A, Vincent J J, Crowley M, Tsui V, Radmer R, Duan Y, Pitera J, Massova I, Seibel G L, Singh U C, Weiner P and Kollman P A 1999 *AMBER 6* (San Francisco, CA: University of California)
[13] Jorgensen W L, Chandrasekhar J, Madura J D, Impey R W and Klein M L 1983 *J. Chem. Phys.* **79** 926
[14] Darden T, York D and Pedersen L 1993 *J. Chem. Phys.* **98** 10089
[15] Essmann U, Perera L, Berkowitz M L, Darden T, Lee H and Pedersen L G 1995 *J. Chem. Phys.* **103** 8577
[16] Ryckaert J P, Ciccotti G and Berendsen H J C 1977 *J. Comput. Phys.* **23** 327
[17] Berendsen H J C, Postma J P M, van Gunsteren W F, DiNola A and Haak J R 1984 *J. Chem. Phys.* **81** 3684
[18] Conway B E 1981 *Ionic Hydration in Chemistry and Biophysics* (Amsterdam: Elsevier Scientific) (distributors for the US and Canada, Elsevier/North-Holland)
[19] Arsic J, Kaminski D M, Radenovic N, Poodt P, Graswinckel W S, Cuppen H M and Vlieg E 2004 *J. Chem. Phys.* **120** 9720
[20] Stöckelmann E and Hentschke R 1999 *J. Chem. Phys.* **110** 12097
[21] Plendl J N and Gielisse P J 1964 *Appl. Opt.* **3** 943
[22] Guillot B 1991 *J. Chem. Phys.* **95** 1543
[23] Robertson C W and Williams D 1971 *J. Opt. Soc. Am.* **61** 1316
[24] Toukan K, Ricci M A, Chen S-H, Loong C-K, Price D L and Teixeira J 1988 *Phys. Rev.* A **37** 2580
[25] Madden P A and Impey R W 1986 *Chem. Phys. Lett.* **123** 502
Silvestrelli P L, Bernasconi M and Parrinello M 1997 *Chem. Phys. Lett.* **277** 478
[26] Zelsmann H R 1995 *J. Mol. Struct.* **350** 95